Article

Concentration control of volatile organic compounds by ionic liquid absorption and desorption☆

Xiaobin Ma [1], Minyan Wu [1], Shuo Liu [2], Jinxing Huang [2], Bin Sun [1], Ying Zhou [1], Qiulian Zhu [1], Hanfeng Lu [1,*]

[1] Institute of Catalytic Reaction Engineering, College of Chemical Engineering, Zhejiang University of Technology, Hangzhou 310014, China
[2] Hangzhou Runxin Technology Co. Ltd., Hangzhou 310014, China

A B S T R A C T

Volatile organic compounds (VOCs) are difficult to be eliminated safely and effectively because of their large concentration fluctuations. Thus, maintaining a stable concentration of VOCs is a significant study. In this research, H_2O, Tween-80, $[Emim]BF_4$, $[Emim]PF_6$, and $[Hnmp]HSO_4$ were applied to absorb and desorb simulated VOCs. The ionic liquid $[Emim]BF_4$ demonstrated the best performance and was thus selected for further experiments. As the ionic liquid acted as a buffer, the toluene concentration with a fluctuation of 2000–20000 mg·m^{-3} was stabilized at 6000–12000 mg·m^{-3}. Heating distillation (90 °C) was highly efficient to recover $[Emim]BF_4$ from toluene. The regenerated $[Emim]BF_4$ could retain its initial absorption capacity even after multiple cycles. Moreover, $[Emim]BF_4$ had the same buffer function on various aromatic hydrocarbons.

1. Introduction

The production process in the chemical industry (paints, glues, fine chemicals synthesis, *etc.*) is a major source of volatile organic compounds (VOCs) [1–3]. Batch reactors are often used in many industrial processes, and the concentration of VOCs emitted from these reactors fluctuates extremely [4]. This large concentration fluctuation limits the safety and efficiency of VOC treatment equipment. Organic gases with reactive activities in exhaust gas, such as aromatics, aldehydes, and olefins, can easily break through the explosion limit and have a fatal impact on the entire plant [5].

Currently, the methods used to control the concentration of VOC emissions can be classified into three categories: gas cabinet, solid absorbent, and liquid absorbent. The gas cabinet uses its large volume to store and buffer organic exhaust gas, but it is a serious safety hazard. Solid absorbents include activated carbon [6], molecular sieves [7,8], silica gel [9], and so on. Activated carbon is the most widely used solid absorbent, but it still has certain disadvantages. For example, some functional groups containing aldehydes, ketones, and esters can destroy its surface structure, causing blockage in the internal pore structure. This phenomenon reduces the adsorption capacity and affects the service life of activated carbon [10]. In addition, the adsorption of activated carbon is an exothermic process, and it becomes extremely easy to burn when the concentration

of VOCs is increased. Therefore, solid absorbents have a large limitation in regulating high concentrations of VOCs [11]. The types of organic solvents used in VOC absorption include vegetable oils [12], silicone oil water emulsions [13,14], di-(2-ethylhexyl) adipate, diisobutyl phthalate [15], poly(ethylene glycol) [16], and oxyethylene sorbitan monooleate [17]. At present, absorbents generally have problems of low absorption capacity and low economic recovery rate. An absorbent is generally recovered by heating distillation accompanying the secondary pollution of the absorbent [18]. Therefore, absorbents with low volatility and high thermal stability and recyclability are urgently needed.

Ionic liquids (ILs) normally composed of organic cations and either organic or inorganic anions are environmental-friendly solvents, which are also called low-temperature molten salts [19,20]. Given their extremely low volatility, ILs can effectively solve the pollution problem caused by the evaporation of absorbents. In addition, ILs can be desorbed and recycled at low temperatures because of their thermal stability [21,22]. Imidazole ILs have attracted considerable attention because of their stable property and simple preparation [23]. At present, many studies used ILs to absorb alkanes [24,25], olefins [26–28], toluene [29], and dichloromethane [30]. When the anions of imidazole ILs are constant, the solubility of VOCs in ILs increases with the increasing length of the cationic alkyl side chain. Anions also have a great influence on the solubility of VOCs. The order of common anion solubility is roughly $[Tf_2N]^- > [CF_3SO_3]^- > [DCA]^- > [BF_4]^- > [Br]^-$.

Although long alkyl side chains can enlarge the solubility of VOCs, they can also increase IL viscosity and limit gas–liquid mass transfer [31]. Thus, in the present work, the common cation $[Emim]^+$ with a short alkyl side chain was selected as part of the candidate IL. The

commonly available and less expensive $[BF_4]^-$ and $[PF_6]^-$ were selected as the anions. Water, Tween-80, and the ILs $[Emim]BF_4$, $[Emim]PF_6$, and $[Hnmp]HSO_4$ were used as the solvents for the capture of VOCs with toluene as a model VOC. The IL $[Emim]BF_4$ showed the best absorption effect and thus was selected for further concentration adjustment experiments. The feasibility of controlling the concentration of VOCs by IL absorption and desorption is proposed.

2. Experimental

2.1. Materials and methods

An N-methylimidazole solution (0.4 mol) was stirred with a magnetic stirrer. Ethyl bromide (0.5 mol) was slowly added dropwise with a constant pressure funnel and refluxed at 70 °C for 8 h. After all the reactants turned into white solids, the reaction was stopped and cooled down to room temperature to obtain a crude intermediate of 1-ethyl-3-methylimidazolium bromide. The obtained solid samples were washed with ethyl acetate twice to remove the soluble residues and steamed at 55 °C for 30 min.

The synthesis of 1-ethyl-3-methylimidazolium tetrafluoroborate was conducted in a round-bottom flask where the intermediate (0.1 mol), sodium tetrafluoroborate ($NaBF_4$, 0.1 mol), and a small amount of acetone were mixed at room temperature for 10 h with a magnetic stirrer. The obtained solution was washed with ethyl acetate twice to remove the soluble residues and then steamed at 55 °C for 30 min. Finally, the IL 1-ethyl-3-methylimidazolium tetrafluoroborate was obtained.

The synthesis of 1-ethyl-3-methylimidazolium hexafluorophosphate was conducted in a round-bottom flask where the intermediate (0.1 mol), sodium hexafluorophosphate ($NaPF_6$, 0.1 mol), and a small amount of acetone were mixed at room temperature for 10 h with a magnetic stirrer. The obtained solution was washed with ethyl acetate twice to remove the soluble residues and then steamed at 55 °C for 30 min. The IL 1-ethyl-3-methylimidazolium hexafluorophosphate was obtained.

A typical synthesis was conducted as follows: in the absence of a solvent, 1-methyl-2-pyrrolidone (0.1 mol) was added to a round-bottom flask. Then, a stoichiometric amount of concentrated sulfuric acid (98%, 0.1 mol) was added dropwise at 0 °C, and the mixture was stirred for 1 h at 0 °C and then stirred for 24 h at room temperature [32]. The IL $[Hnmp]HSO_4$ was washed repeatedly with ethyl acetate to remove nonionic residues and dried under vacuum.

A representative surfactant, Tween-80 (polyoxyethylene sorbitan monooleate), was selected as a comparative sample. A Tween-80 solution having a mass fraction of 25 ppm and deionized water as an absorbent control were disposed.

2.2. Characterization

Fourier transform infrared (FTIR) spectra were obtained by the KBr method, recorded on a Bruker Vertex 70 infrared spectrometer, and scanned from 4000 cm^{-1} to 500 cm^{-1}.

The viscosity of the absorbent was directly read by using the Lichen Technology NDJ-1 Rotating Viscometer with different rotors.

The water content of ILs was determined by the W/A-1C moisture analyzer.

2.3. Determination of Henry's constant

2.3.1. Theoretical development

Dimensionless Henry's constant H was obtained using a static method [33]. The theoretical development is shown as follows:

The static headspace method requires that chemical and thermal equilibria are achieved within the enclosed sampling vessel when solutes are present at low concentrations. The ratio of the concentration of volatile components in the gas–liquid phase is defined as Henry's constant (Eq. (1))

$$H = \frac{C_g}{C_w} \tag{1}$$

where C_g is the equilibrium concentration (mol·L^{-1}) of the component in the vapor phase and C_w is the equilibrium concentration (mol·L^{-1}) of the component in the liquid phase.

In a closed system, the component mass balance equation can be expressed as Eq. (2):

$$C_0 V_w = C_g V_g + C_w V_w \tag{2}$$

where C_0 is the initial concentration (mol·L^{-1}) of the component in the vapor phase, and V_w and V_g are the volumes (m^3) of the vapor and liquid phases.

Both sides of the equation are divided by V_w to obtain Eq. (3).

$$C_0 = \frac{C_g V_g}{V_w} + C_W \tag{3}$$

Further available:

$$C_0 = C_g \left(\frac{V_g}{V_w} + K \right) \tag{4}$$

where K is the reciprocal of Henry's constant. Let $V_g/V_w = R$ be the gas–liquid, and further simplification yields Eq. (5).

$$\frac{1}{C_g} = \frac{K + R}{C_0} \tag{5}$$

According to the chromatographic principle, the concentration of the component is proportional to the peak area of the chromatogram.

$$C_g = fA \tag{6}$$

Substituting Eq. (6) into Eq. (5) and rearranging gives

$$\frac{1}{A} = \frac{fK}{C_0} + \frac{fR}{C_0} \tag{7}$$

where A is the headspace peak area and f is the chromatographic correction factor. The formula shows that a straight line can be obtained by plotting the reciprocal area of the chromatographic peak area $(1/A)$ against the gas–liquid ratio (R).
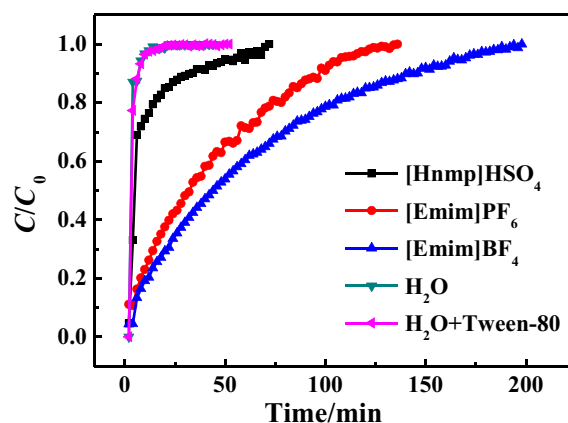
$$y = ax + b \tag{8}$$

Fig. 1. Experimental breakthrough curves of toluene on five absorbents ($v = 100$ ml·min^{-1}, $T = 30$ °C, inlet toluene concentration 12000 mg·m^{-3}).

Table 1
Physical properties of five absorbents at 30 °C

Ionic liquid	Viscosity/mPa·s	Henry's constant $\times 10^3$	Absorption/ mg·g^{-1}	H_2O/%	Br/%
[Hnmp]HSO$_4$	1600	32	1.5	–	–
[Emim]BF$_4$	30	24	4.5	0.36	11
[Emim]PF$_6$	26	30	3.5	0.47	8.9
Tween-80	0.9	–	0.28	–	–
H$_2$O	0.9	680	0.23	–	–

In the formula, $a = f/C_0$, and $b = f \cdot k/C_0$. The slope a and the intercept b were calculated. Finally, Henry's constant of the component was obtained.

$$H = \frac{a}{b} \tag{9}$$

2.3.2. Methods

A known quantity of solvent IL was placed in a specific flask (vial), whose exact volume was measured. The flask was gas-tightly sealed
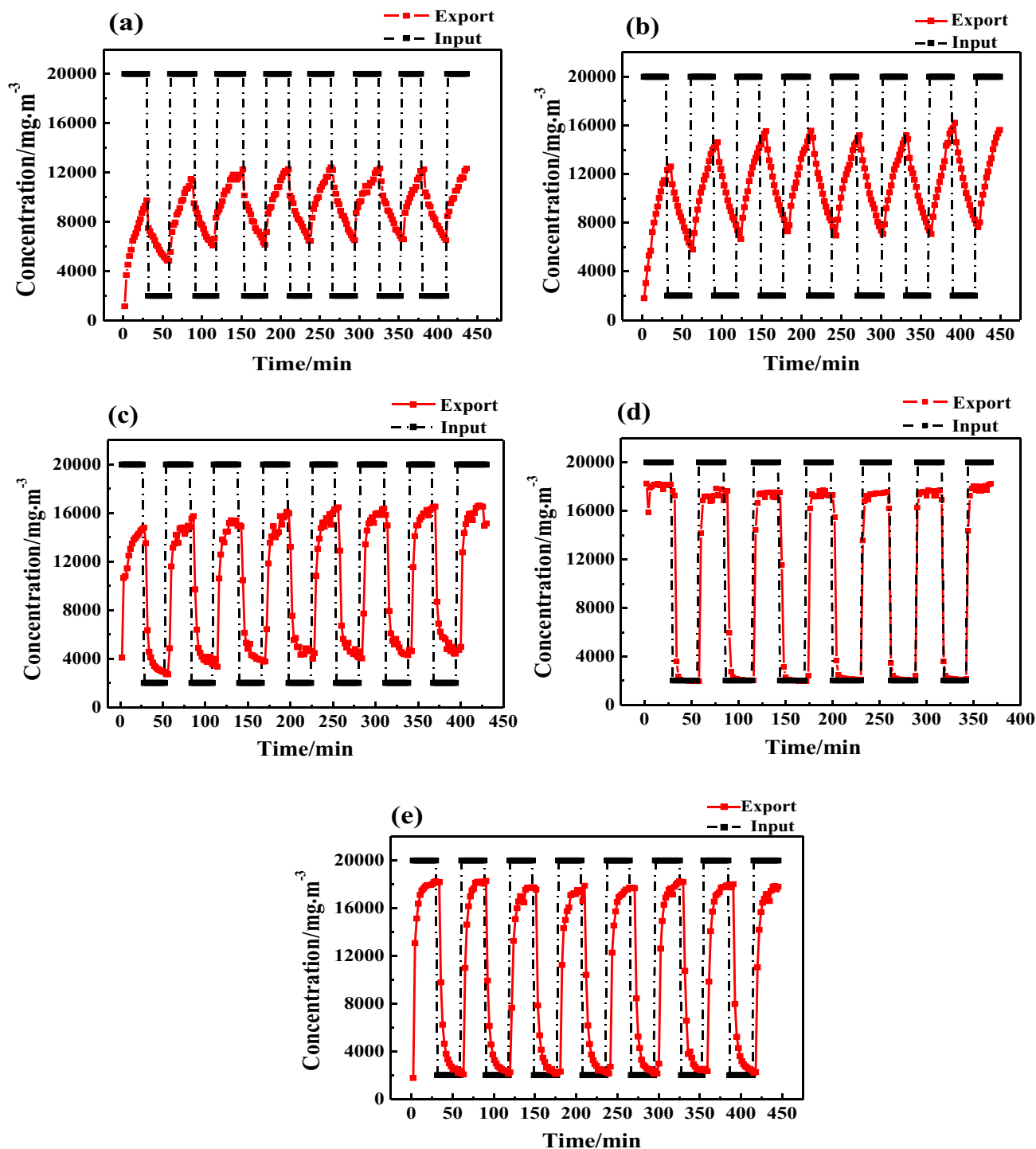

Fig. 2. Absorption performance of five absorbents on toluene with concentration fluctuations. ($v = 100$ ml·min^{-1}, $T = 30$ °C, toluene concentration changed every 30 min from 20000 mg·m^{-3} to 2000 mg·m^{-3}) (a): [Emim]BF$_4$, (b): [Emim]PF$_6$, (c): [Hnmp]HSO$_4$, (d): water, (e): Tween-80 aqueous solution.

and then added with a known quantity of VOC through the septum. For example, 3 μl of toluene was dissolved in 7 ml of IL, and four 10 ml head-space bottles were added to 0.5 ml, 1 ml, 2 ml, and 2.5 ml of the same test solution. The gas–liquid ratios in the headspace were 19, 9, 4, and 3, respectively. The headspace bottles were sealed with silicone rubber pad and rolled with aluminum cover. The bottles containing the sample were placed in a 30 °C water bath for 1 h. After equilibration, 1 ml of the headspace gas was extracted with a 1 ml gas-tight sampler and analyzed by gas chromatography. Finally, Henry's constant was determined.

2.4. Absorption performance test

Toluene, a typical aromatic hydrocarbon, was selected as the representative VOC because of its wide industrial applications and hazardous impacts on the environment. Gaseous toluene was generated by bubbling liquid toluene at 0 °C with standard air flow. The flow volume was regulated by a mass flow controller. The generated gaseous toluene was transferred to a buffer by air and then diluted with air at the required concentration. The inlet toluene concentration was controlled at 12000 mg·m^{-3}. The total flow rate was 100 ml·min^{-1}. The gaseous toluene was then passed through an absorption column at 30 °C. The column 20 in diameter and 34.5 mm in height contained 10 g of the absorbent. The inlet and outlet toluene concentrations were monitored online by an Agilent 6890 gas chromatograph equipped with a flame ionization detector. Absorption capacity was calculated according to Eq. (10)

$$q = \frac{F \times C_0 \times 10^{-9}}{W} \left[t_s - \int_0^{t_s} \frac{C_i}{C_0} dt \right] \tag{10}$$

where q is the equilibrium absorption capacity (mg·g^{-1}); F is the flow volume of the carrier gas (air) (100 ml·min^{-1}), t_s is the time to reach absorption equilibrium (min), W is the mass of the absorbent (g), C_0 is the inlet concentration of the adsorbed gas (mg·m^{-3}), and C_i is the outlet concentration of the adsorbed gas (mg·m^{-3}).

3. Results and Discussion

3.1. Absorption of toluene in different solvents

Toluene was used as a model. Fig. 1 shows the toluene dynamic absorption breakthrough curves of the five types of absorbents. The curves can be divided into two stages. During the first stage, the outlet concentration of toluene increased significantly with the increase in absorption time, and the toluene concentration gradually reached the breakthrough point. In the second stage, the outlet concentration reached saturation and basically no longer changed with time. This absorption law can be explained by the principle of gas–liquid equilibrium of the system. During the absorption process, the toluene in the exhaust gas mass transfers to the absorbent, and the mass transfer of toluene molecules in the liquid phase to the gas phase simultaneously occurs. When the concentration of toluene in the absorbent reaches a certain ratio with the concentration of toluene in the exhaust gas, the mass transfer rate of the absorption process becomes equal to that of the desorption process. The gas–liquid phase also reaches a dynamic equilibrium (saturated absorption). Toluene in the exhaust gas is no longer absorbed by the absorbent. Among all the absorbents, IL [Emim]BF$_4$ and deionized water exhibited the longest (i.e., reached 180 min) and shortest (i.e., only 12 min) breakthrough times, respectively.

To clarify the possible mechanisms for absorption toluene using the ionic liquids, conductor-like-screening model for real solvent (COSMO-RS) method was used to analyze the solute–solvent interaction of toluene on hundreds of ILs [34–37]. It is observed that the toluene absorption capacity of ILs is determined by the selection of both cationic and anionic structures. Long chain imidazolium cations and tetra-

substituted long chain phosphonium or ammonium cations seem to improve the capacity for absorbing toluene. Increasing the length of the alkyl group essentially increases the non-polar character of the ILs, which enhance the solubility of toluene in ILs. On the other hand, the highly halogenated hydrophobic anions such as $[C_6F_{18}P]^-$, $[Tf_2N]^-$, and $[FeCl_4]^-$ also improve the absorption of toluene [37]. Since the anion $[BF_4]^-$ halogenation is higher than $[PF_6]^-$, [Emim]BF$_4$ has better performance than [Emim]PF$_6$.

Table 1 lists the physical properties of each absorbent at 30 °C. As shown in the table, the smaller the Henry's constant of the absorbent to toluene, the higher the absorption. However, [Hnmp]HSO$_4$ with the low Henry's constant has a poor absorption of toluene due to its high viscosity reaching 1600 mPa·s. In accordance with two-film theory [29], when the gas phase toluene molecule is in contact with the absorbent, a phase interface is formed between the two phases. In addition, a flowable layered gas film and a liquid film exist on both sides of the phase interface. The toluene molecules must pass through the two layers in a molecular diffusion manner. Given that the concentration of toluene in the gas and liquid phases is different, a certain concentration gradient provides power for the diffusion. However, diffusion resistance occurs between the two films, and the viscosity of the absorbent plays a key role in the magnitude of this resistance. The lower the viscosity of the absorbent, the smaller its intramolecular internal frictional resistance; thus, the toluene has less resistance to enter the absorbent. This phenomenon results in improved absorption effect. The opposite scenario results in poor absorption effect.

Fig. 2 shows that the concentration of the five absorbents of toluene changed from 20000 mg·m^{-3} to 2000 mg·m^{-3} per 30 min. The curves can also be divided into two stages. First, when the inlet gas was 20000 mg·m^{-3}, the outlet gas increased with time. When the inlet gas concentration dropped to 2000 mg·m^{-3}, the outlet gas decreased. After 150 min of absorption, the concentration of the outlet gas basically stabilized and changed regularly with time. The difference of each absorbent was mainly reflected in the fluctuation of the outlet gas concentration with time. When the absorbent was [Emim]BF$_4$, the outlet gas concentration fluctuated less than the other four absorbents. Finally, the concentration can be stabilized at 6000–12000 mg·m^{-3}. The effect of concentration adjustment was realized. [Emim]PF$_6$ effect was second, and that of [Hnmp]HSO$_4$ was not ideal due to its large viscosity. Water and Tween-80 aqueous solution caused no adjustment effect.

3.2. [Emim] BF$_4$ absorption of toluene in different conditions

When the IL absorbed different concentrations of toluene, its absorption rate was almost unchanged (Fig. 3). According to the two-film theory [29], toluene molecules must pass through the gas–liquid interface
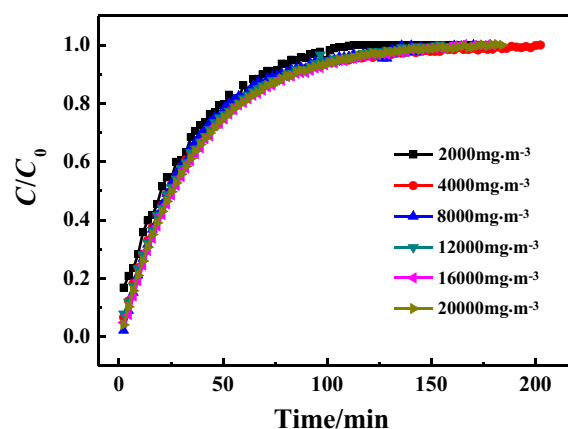

Fig. 3. Experimental breakthrough curves of toluene at different concentrations ($v = 100$ ml·min^{-1}, $T = 30$ °C).

to be dissolved in the IL phase. With the increase in toluene concentration, the concentration gradient of the gas–liquid phase increased, which improved the mass transfer driving force. This effect benefited the absorption of toluene in the ILs and enhanced the absorptivity. Therefore, when toluene at a high concentration entered the IL, the IL absorbed part of the toluene to reduce the high concentration. When toluene at a low concentration entered the IL, the IL released the absorbed part of the toluene to enhance the concentration.

The relationship between temperature and absorptivity was studied at temperature intervals of 30 °C, 60 °C, and 90 °C. As shown in Fig. 4(b),

the absorptivity decreased with increasing temperature. When the temperature was raised, Henry's constant increased [33]. And it consequently decreases the solubility of toluene in the ILs. As shown in Fig. 4(c), the saturated absorption isotherm of toluene absorbed by [Emim]BF$_4$ from 30 °C and 90 °C in this apparatus was reduced from 4.5 mg·g^{-1} to 0.0045 mg·g^{-1}. Fig. 4(a) shows that over the same range, the viscosity of the IL reduced and the dissolution capacity for toluene strengthened [18]. Unfortunately, the latter contribution cannot offset the decrease in removal efficiency. These results indicate that 30 °C is the optimal temperature for absorbing toluene in the ILs.

3.3. IL recycling performance

From an economic point of view, the ability to regenerate the IL for reuse is an important factor for industrial applications because regeneration reduces reagent costs in removing VOCs. As shown in Fig. 4(b), the low absorption characteristic of IL at high temperature was used to desorb the gas. As shown in Fig. 5(a), the solubility of toluene after three cycles was basically unchanged. The FTIR spectra of the fresh and used ILs are shown in Fig. 5(b). The broad bands observed at 3000–3700 and 2900 cm^{-1} corresponded to O—H (hydroxyl or carboxyl groups) and aliphatic C—H stretching vibrations, respectively [38]. Alkyl group chain substituted C—H stretching vibrations at 2967 cm^{-1}, 2940 cm^{-1}, and 2880 cm^{-1} while the imidazole ring skeleton vibrations at 1574 cm^{-1} and 1470 cm^{-1}. Bands below 1000 cm^{-1} were assigned
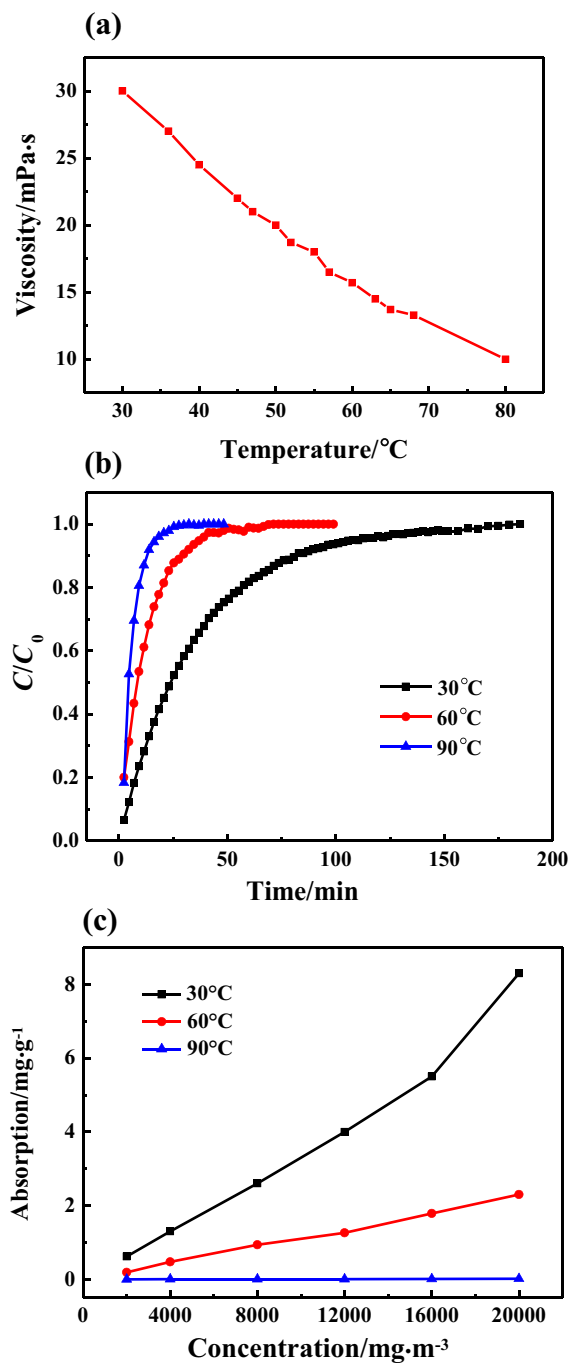

Fig. 4. (a): Viscosity curves of ionic liquid at different temperatures; (b): experimental breakthrough curves of toluene at different temperatures; (c): absorption isotherm of [Emim]BF$_4$ at different temperatures.
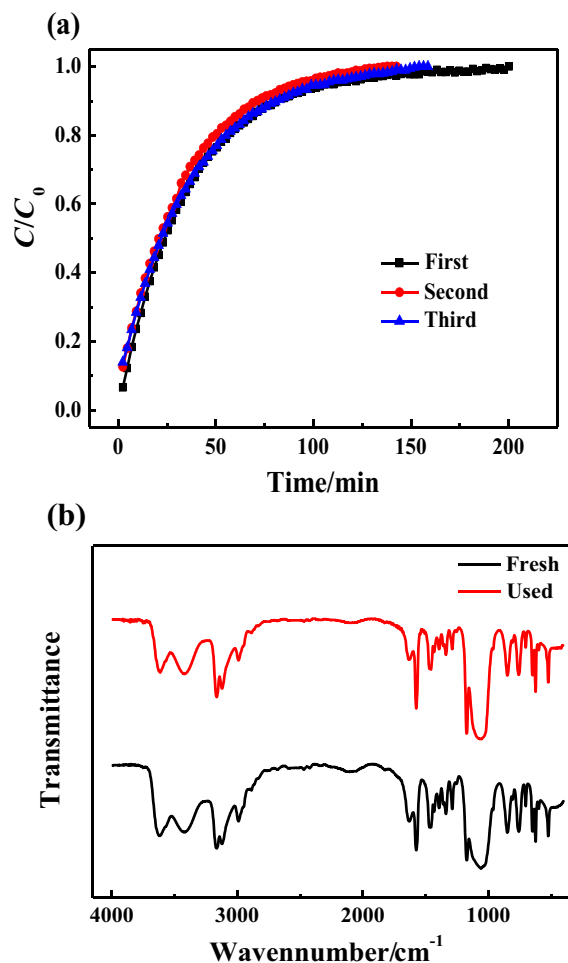

Fig. 5. (a): The effect of cycles on the toluene absorption; (b): the infrared spectrum cures of before and after [Emim]BF$_4$ use.

Table 2
Henry's constant at each temperature

Temperature/°C	Henry's constant
30	0.024
60	0.041
90	0.15

to the out-of-plane bending vibration of the aromatic C—H. Meanwhile, the band at 840 cm^{-1} corresponded to B—F stretching vibration. The structure of the IL was basically unchanged before and after use.

3.4. [Emim] BF$_4$ absorption adsorbs different VOCs

Several representative VOCs were selected in the experiment, and their Henry's constants were measured (Table 2). The measured Henry's constants are basically consistent with their breakthrough curves in the IL. As shown in Fig. 6(a), the smaller the Henry coefficient, the larger the saturated absorption of VOCs in the solution. By comparison, for the same IL, the VOCs containing unsaturated structure had higher solubility than alkanes, such as *n*-hexane. This result may be because the π electrons in the unsaturated structure enhanced the gas solute and IL interaction. The absorption of aromatic hydrocarbons was significantly
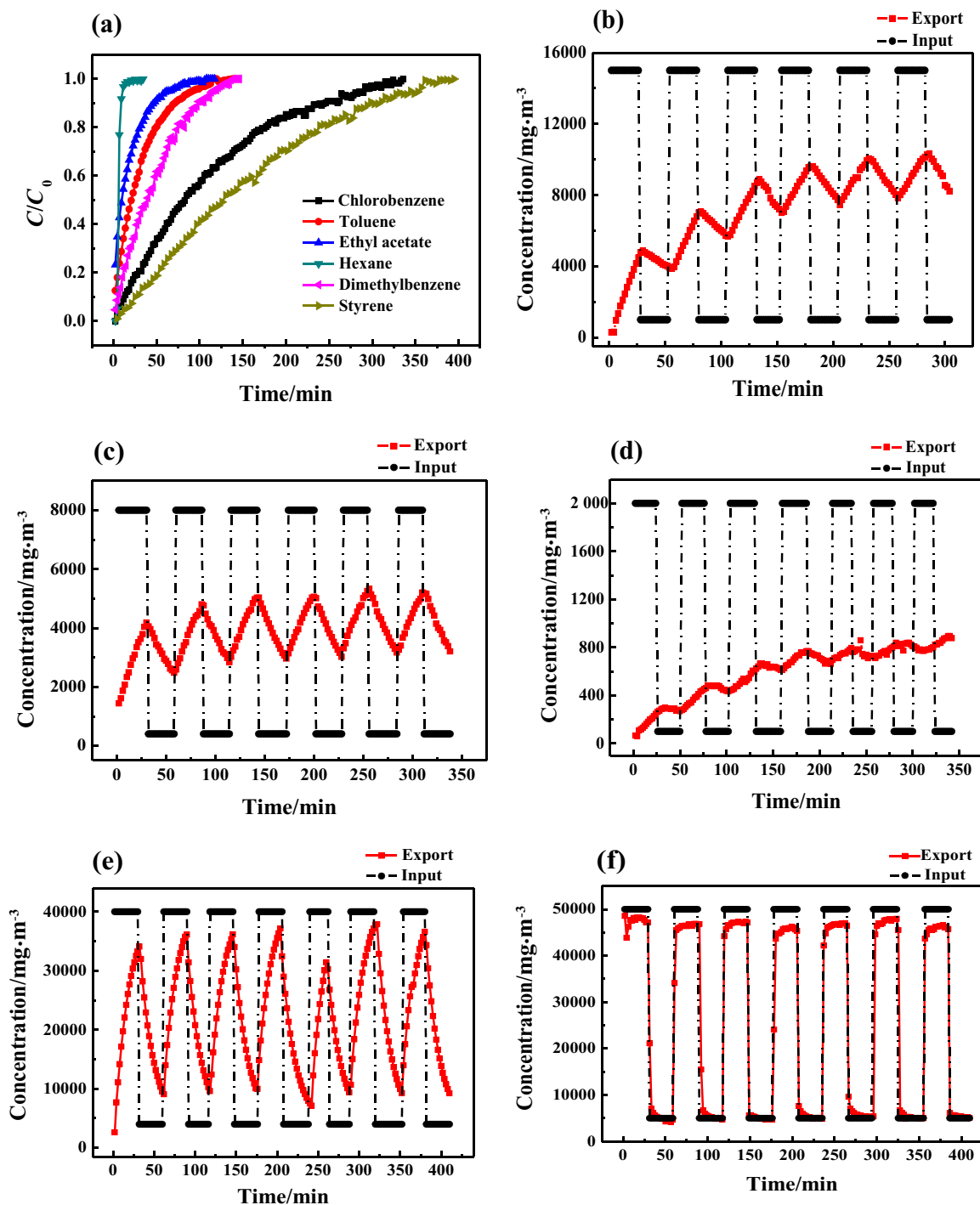
Fig. 6. (a): Experimental breakthrough curves of VOCs on [Emim]BF$_4$ ($v = 100$ ml·min^{-1}, $T = 30$ °C); absorption performance of [Emim]BF$_4$ on VOCs ($v = 100$ ml·min^{-1}, $T = 30$ °C, VOC concentration changed every 30 min); (b): dimethylbenzene; (c): chlorobenzene; (d): styrene; (e): ethyl acetate; (f): *n*-hexane.

Table 3
Physical parameters of each VOC

Ionic liquid	Boiling point/°C	Density/g·ml^{-1}	Polarity	Viscosity/mPa·s	Absorption/mg·g^{-1}	Henry's constant$\times 10^3$
Toluene	110	0.87	Weak	0.59	4.5	24
Dimethylbenzene	138	0.86	Weak	0.65	5.5	19.5
Styrene	146	0.909	Weak	0.725	17.6	1.81
Chlorobenzene	132	1.11	Weak	0.8	12.73	2.4
Ethyl acetate	77	0.90	Polarity	0.45	1.6	120
Hexane	69	0.69	Non-polar	0.33	0.5138	280

higher than that of alkanes. The unsaturated large π bond on the benzene ring possibly interacted with the π-conjugated system in the imidazolium cation, with the π–π bonds of the π electron in the anion, and with the lone pairs of electrons in anions. Fig. 6(b) shows that [Emim]BF$_4$ has a good buffering effect on the adjustment of aromatics concentration fluctuation. However, its regulation is weak for the absorption of alkanes (Table 3).

4. Conclusions

The five absorbents were used to treat the simulated exhaust gas under controlled laboratory conditions. The following conclusions have been drawn:

(1) The IL [Emim]BF$_4$ absorbs VOC gas in accordance with the general application law that the absorption increases with the increase in gas concentration and decreases with increasing temperature.

(2) During the absorption of separation gas, the IL can effectively solve the pollution problem caused by the evaporation of the absorbent. Given their thermal stability, the ILs can be desorbed and recycled at a low temperature.

(3) The IL [Emim]BF$_4$ has a good buffering effect on the adjustment of aromatics concentration fluctuation and has a good reference value for industrial applications. However, further adjustments to the concentration of VOCs in alkanes are needed.

References

[1] M.S. Kamal, S.A. Razzak, M.M. Hossain, Catalytic oxidation of volatile organic compounds (VOCs) — a review, *Atmos. Environ.* 140 (2016) 117–134.

[2] J.Y. Zheng, Y.F. Yu, Z.W. Mo, Z. Z, X.M. Wang, S.S. Yin, K. Peng, Y. Yang, X.Q. Feng, H.H. Cai, Industrial sector-based volatile organic compound (VOC) source profiles measured in manufacturing facilities in the Pearl River Delta, China, *Sci. Total Environ.* 456-457 (2013) 127–136.

[3] X. Chen, Z.L. Zhao, Y. Zhou, Q.L. Zhu, Z.Y. Pan, H.F. Lu, A facile route for spraying preparation of Pt/TiO$_2$ monolithic catalysts toward VOCs combustion, *Appl. Catal. A Gen.* 566 (2018) 190–199.

[4] B. Srinivasan, S. Palanki, D. Bonvin, Dynamic optimization of batch processes: I. Characterization of the nominal solution, *Comput. Chem. Eng.* 27 (2003) 1–26.

[5] C.M. Shu, P.J. Wen, Investigation of the flammability zone of o-xylene under various pressures and oxygen concentrations at 150 °C, *J. Loss Prev. Process Ind.* 15 (2002) 253–263.

[6] H.Y. Zhao, X.A. Lu, Y. Wang, B. Sun, X.H. Wu, H.F. Lu, Effects of Additives on Sucrose-derived Activated Carbon Microspheres Synthesized by Hydrothermal Carbonization, Chemical Routes to Materials 52(2017) 10787–10799.

[7] Y. Ueno, A. Tate, O. Niwa, H.S. Zhou, T. Yamada, I. Honma, High benzene selectivity of mesoporous silicate for BTX gas sensing microfluidic devices, *Anal. Bioanal. Chem.* 382 (2005) 804–809.

[8] C. Yuan, H.Y. Liu, Z.K. Zhang, H.F. Lu, Q.L. Zhu, Y.F. Chen, Alkali-metal-modified ZSM-5 zeolites for improvement of catalytic dehydration of lactic acid to acrylic acid, *Chin. J. Catal.* 36 (2015) 1861–1866.

[9] H.N. Wang, M. Tang, K. Zhang, D.F. Cai, W.Q. Huang, R.Y. Chen, C.Z. Yu, Functionalized hollow siliceous spheres for VOCs removal with high efficiency and stability, *J. Hazard. Mater.* 268 (2014) 115–123.

[10] X.Y. Zhang, B. Gao, A.E. Creamer, C.C. Cao, Y.C. Li, Adsorption of VOCs onto engineered carbon materials: A review, *J. Hazard. Mater.* 338 (2017) 102–123.

[11] K. Urashima, J.S. Chang, Removal of volatile organic compounds from air streams and industrial flue gases by non-thermal plasma technology, *IEEE Trans. Dielectr. Electr. Insul.* 7 (2000) 602–614.

[12] B. Ozturk, D. Yilmaz, Absorptive removal of volatile organic compounds from flue gas streams, *Process. Saf. Environ. Prot.* 84 (2006) 391–398.

[13] E. Dumont, G. Darracq, A. Couvert, C. Couriol, A. Amrane, D. Thomas, Y. Andrès, P.L. Cloirec, Hydrophobic VOC absorption in two-phase partitioning bioreactors;

[14] R. Tatin, L. Moura, N. Dietrich, S. Baig, G. Hébrard, Physical absorption of volatile organic compounds by spraying emulsion in a spray tower: Experiments and modelling, *Chem. Eng. Res. Des.* 104 (2015) 409–415.

[15] F. Heymes, P.M. Demoustier, F. Charbit, J.L. Fanlo, P. Moulin, Recovery of toluene from high temperature boiling absorbents by pervaporation, *J. Membr. Sci.* 284 (2006) 145–154.

[16] F. Cotte, J.L. Fanlo, P.L. Cloirec, P. Escobar, Absorption of odorous molecules in aqueous solutions of polyethylene glycol, *Environ. Technol.* 16 (1995) 127–136.

[17] B. Park, G. Hwang, S. Haam, C. Lee, I.S. Ahn, K. Lee, Absorption of a volatile organic compound by a jet loop reactor with circulation of a surfactant solution: Performance evaluation, *J. Hazard. Mater.* 153 (2008) 735–741.

[18] W.L. Wang, X.L. Ma, S. Grimes, H.F. Cai, M. Zhang, Study on the absorbability, regeneration characteristics and thermal stability of ionic liquids for VOCs removal, *Chem. Eng. J.* 328 (2017) 353–359.

[19] K.R. Seddon, Ionic liquids: A taste of the future, *Nat. Mater.* 2 (2003) 363–365.

[20] G. Quijano, A. Couvert, A. Amrane, G. Darracq, C. Couriol, P.L. Cloirec, L. Paquin, D. Carrié, Toxicity and biodegradability of ionic liquids: New perspectives towards whole-cell biotechnological applications, *Chem. Eng. J.* 174 (2011) 27–32.

[21] C.F. Poole, S.K. Poole, Extraction of organic compounds with room temperature ionic liquids, *J. Chromatogr. A* 1217 (2010) 2268–2286.

[22] P.F. Zhang, H.F. Lu, Y. Zhou, L. Zhang, Z.L. Wu, H.L. Shi, Q.L. Zhu, Y.F. Chen, S. Dai, Mesoporous MnCeOx solid solutions for low temperature and selective oxidation of hydrocarbons, *Nat. Commun.* 6 (2015) 8846.

[23] G. Quijano, A. Couvert, A. Amrane, G. Darracq, C. Couriol, P.L. Cloirec, L. Paquin, D. Carrié, Potential of ionic liquids for VOC absorption and biodegradation in multiphase systems, *Chem. Eng. Sci.* 66 (2011) 2707–2717.

[24] J. Jacquemin, M.F.C. Gomes, P. Husson, V. Majer, Solubility of carbon dioxide, ethane, methane, oxygen, nitrogen, hydrogen, argon, and carbon monoxide in 1-butyl-3-methylimidazolium tetrafluoroborate between temperatures 283 K and 343 K and at pressures close to atmospheric, *J. Chem. Thermodyn.* 38 (2006) 490–502.

[25] J. Kumełan, A.P.S. Kamps, D. Tuma, G. Maurer, Solubility of the single gases methane and xenon in the ionic liquid [bmim][CH$_3$SO$_4$], *J. Chem. Eng. Data* 52 (2007) 2319–2324.

[26] D. Camper, C. Becker, C. Koval, R. Noble, Diffusion and solubility measurements in room temperature ionic liquids, *Ind. Eng. Chem. Res.* 45 (2006) 445–450.

[27] D. Camper, C. Becker, C. Koval, R. Noble, Bulk-fluid solubility and membrane feasibility of Rmim-based room-temperature ionic liquids, *Ind. Eng. Chem. Res.* 45 (2006) 6279–6283.

[28] R. Condemarin, P. Scovazzo, Gas permeabilities, solubilities, diffusivities, and diffusivity correlations for ammonium-based room temperature ionic liquids with comparison to imidazolium and phosphonium RTIL data, *Chem. Eng. J.* 147 (2009) 51–57.

[29] T. Nguyen, A.S.R. Castillo, S. Guihéneuf, P.F. Biard, L. Paquin, A. Amrane, A. Couvert, Toluene degradation in a two-phase partitioning bioreactor involving a hydrophobic ionic liquid as a non-aqueous phase liquid, *Int. Biodeterior. Biodegrad.* 117 (2017) 31–38.

[30] V. Najdanovic-Visak, A. Rodriguez, Z.P. Visak, J.N. Rosa, C.A.M. Afonso, M.N. Ponte, L.P.N. Rebelo, Co-solvent effects in LLE of 1–hydroxyethyl–3–methylimidazolium based ionic liquids plus 2-propanol plus dichloromethane or 1,2-dichloroethane, *Fluid Phase Equilib.* 254 (2007) 35–41.

[31] E. Dumont, Y. Andres, P.L. Cloirec, Effect of organic solvents on oxygen mass transfer in multiphase systems: Application to bioreactors in environmental protection, *Biochem. Eng. J.* 30 (2006) 245–252.

[32] B.H. Huang, Y.F. Wang, K. Mang, Y.X. Fang, B.L. Zhou, Synthesis of pyrrolidonium acidic ionic liquids and their catalytic activity for esterification of acetic acid and butanol, *Chin. J. Catal.* 28 (2007) 743–748.

[33] M.D. Vuong, A. Couvert, C. Couriol, A. Amrane, P.L. Cloirec, C. Renner, Determination of the Henry's constant and the mass transfer rate of VOCs in solvents, *Chem. Eng. J.* 150 (2009) 426–430.

[34] Q.W. Yang, D. Xu, Z.B. Bao, Y. Zhang, B.G. Su, Q.L. Ren, H.B. Xing, Design and screening of ionic liquids for C$_2$H$_2$/C$_2$H$_4$ separation by COSMO-RS and experiments, *AIChE J.* (6) (2015) 2016–2027.

[35] Y. Zhang, X. Zhao, Z.Q.W. Yang, Z.G. Zhang, Q.L. Ren, H.B. Xing, Long-chain carboxylate ionic liquids combining high solubility and low viscosity for light hydrocarbon separations, *Ind. Eng. Chem. Res.* 56 (2017) 7336–7344.

[36] Q.W. Yang, Z.Q. Zhang, X.G. Sun, Y.S. Hu, H.B. Xing, S. Dai, Ionic liquids and derived materials for lithium and sodium batteries, *Chem. Soc. Rev.* 47 (2018) 2020–2064.

[37] J. Bedia, E. Ruiz, J.D. Riva, V.R. Ferro, J. Palomar, J.J. Rodriguez, Optimized ionic liquids for toluene absorption, *AIChE J.* 59 (2013) 1648–1656.

[38] M. Sevilla, A.B. Fuertes, Chemical and structural properties of carbonaceous products obtained by hydrothermal carbonization of saccharides, *Chemistry Weinheim Bergstr. Germ.* 15 (2009) 4195–4203.